
The Underlying Scaling Laws and Universal Statistical Structure of Complex Datasets

Noam Levi and Yaron Oz

Raymond and Beverly Sackler School of Physics and Astronomy
Tel-Aviv University
Tel-Aviv 69978, Israel
noam@mail.tau.ac.il

Abstract

We study universal traits which emerge both in real-world complex datasets, as well as in artificially generated ones. Our approach is to analogize data to a physical system and employ tools from statistical physics and Random Matrix Theory (RMT) to reveal their underlying structure. We focus on the feature-feature covariance matrix, analyzing both its local and global eigenvalue statistics. Our main observations are: (i) The power-law scalings that the bulk of its eigenvalues exhibit are vastly different for uncorrelated random data compared to real-world data, (ii) this scaling behavior can be completely recovered by introducing long range correlations in a simple way to the synthetic data, (iii) both generated and real-world datasets lie in the same universality class from the RMT perspective, as chaotic rather than integrable systems, (iv) the expected RMT statistical behavior already manifests for empirical covariance matrices at dataset sizes significantly smaller than those conventionally used for real-world training, and can be related to the number of samples required to approximate the population power-law scaling behavior, (v) the Shannon entropy is correlated with local RMT structure and eigenvalues scaling, and substantially smaller in strongly correlated datasets compared to uncorrelated synthetic data, and requires fewer samples to reach the distribution entropy. These findings can have numerous implications to the characterization of the complexity of data sets, including differentiating synthetically generated from natural data, quantifying noise, developing better data pruning methods and classifying effective learning models utilizing these scaling laws.

1 Introduction

In recent years, very large models have achieved state-of-the-art performance on both supervised and unsupervised learning tasks. These models often lie outside the regimes of classical machine learning (under-parameterized) and deep learning (over-parameterized), but rather in the limit where both the number of parameters and the number of samples are extremely large. While the behavior of these complex models can be challenging to predict, it has been observed that successively scaling up the number of parameters, dataset size, and compute power, continuously improve performance according to a power-law scaling, as long as the model isn't bottlenecked by any of the other two. Several studies have been conducted to understand the origin of this power-law scaling behavior [1, 2], deducing that it may lie in the way that neural networks transform features in the data, which in turn extends the power-law behavior from the data to the loss function.

In this work, we continue the investigation of the relationship between neural networks and scaling laws. We focus on the source of the scaling laws that manifest in the data itself, rather than on how neural networks extend them. Concretely, we explore the underlying properties that seem to

be universal across many datasets, regardless of origin and complexity. To achieve this goal, we analyze the empirical feature-feature covariance matrix spectrum and attempt to answer the following questions:

- Is power-law scaling a universal property across real-world datasets?; what determines the scaling exponent and what properties should a synthetic dataset have, in order to follow the same scaling?
- What are the universal properties of datasets that can be gleaned from the empirical covariance matrix and how are they related to local and global statistical properties of RMT?
- How to quantify the extent to which an empirical covariance matrix characterize complex data well?
- What, if any, are the relations between datasets scaling, entropy and statistical chaos diagnostics?

We follow two complementary approaches: first, we explore the scaling behavior of the bulk of non-vanishing eigenvalues, and second, we study the distributional properties of the spectrum using tools from statistical physics and Random Matrix Theory (RMT).

RMT is a powerful tool for describing the spectral statistics of certain complex systems. It is particularly useful for systems that are chaotic but also have certain coherent properties. The theory predicts universal statistical structures, provided that the underlying matrix ensemble is large enough to sufficiently fill the space of all matrices with a given symmetry, a property known as ergodicity [3]. Ergodicity has been observed in a variety of systems, including chaotic quantum systems [4–6], financial markets, nuclear physics and many others [7–9]. To demonstrate that a similar universal structure is also observed for correlation matrices resulting from datasets, we will employ several diagnostic tools widely used in the field of quantum chaos. We will analyze the global and local statistics of empirical covariance matrices generated from two classes of datasets: (i) Synthetic, normally distributed samples, with either uncorrelated or correlated features, (ii) Real-world datasets composed of images, at varying levels of complexity and resolution.

Our primary contributions are:

1. We find that power-law scaling appears across various datasets. It is governed by a single scaling exponent α , and its origin is the strength of correlations in the underlying population matrix. We accurately recover the behavior of the eigenvalue bulk of real-world datasets using Wishart matrices with a Toeplitz covariance matrix [10]. We dub these *Synthetic Analogues*.
2. We show that generically, the bulk of eigenvalues’ statistical properties are well described by RMT predictions, verified by diagnostic tools typically used for quantum chaotic systems.
3. We find that the effective convergence of the empirical covariance matrix as a function of the number of samples correlates with the corresponding RMT description becoming a good description of the statistics and the eigenvalues scaling.
4. The Shannon entropy is correlated with the local RMT structure and the eigenvalues scaling, and is substantially smaller in strongly correlated datasets compared to uncorrelated synthetic data. Additionally, it requires fewer samples to reach the distribution entropy.

Our findings offer a new perspective on the properties of both real-world and synthetic datasets and provide a foundation for future work exploring the fundamental properties of these systems. By understanding the underlying properties of the data, we can gain new insights into the behavior of large neural networks, ultimately leading to more efficient and effective models.

2 Background and Related Work

Neural Scaling Laws Neural scaling laws are a set of empirical observations that describe the relationship between the size of a neural network, dataset, compute power, and its performance. These laws were first proposed by Kaplan et al. [1] and have since been confirmed by a number of other studies [2, 11] and studied further in [12–17]. The main finding of neural scaling laws is that the test loss of a neural network scales as a power-law with the number of parameters in the network. This means that doubling the number of parameters roughly reduces the test loss by 2^α . However, this relationship does not persist indefinitely, and there is a point of diminishing returns beyond which increasing the number of parameters does not lead to significant improvements in

performance. One of the key challenges in understanding neural scaling laws is the complex nature of the networks themselves. The behavior of a neural network is governed by a large number of interacting parameters, making it difficult to identify the underlying mechanisms that give rise to the observed scaling behavior, and many advances have been made by appealing to the RMT framework.

Random Matrix Theory RMT is a branch of mathematics that was originally developed to study the properties of large matrices with random entries. It is particularly suited to studying numerous realizations of the same system, where the number of realizations $M \rightarrow \infty$, the dimensions of the system $d \rightarrow \infty$, and the ratio between the two tends to a constant $d/M \rightarrow \text{const.} \leq 1$. Results from RMT calculations have been applied to a wide range of problems in Machine Learning (ML), beyond the scope of neural scaling laws, including the study of nonlinear ridge regression [18], random Fourier feature regression [19], the Hessian spectrum [20], and weight statistics [21]. For a review of some of the recent developments, we refer the reader to Couillet and Liao [22] and references therein.

Internal Statistics of Datasets Understanding the statistical properties of synthetic and real-world datasets has become a subject of growing interest in recent years. As images generated from state of the art models [23–25] become increasingly more accurate and detailed, the ability to make statistical statements regarding the fidelity of data is ever more important [26–28]. Some of the methods commonly employed to distinguish the internal statistics of images include Principal Component Analysis (PCA) [29, 30], Nonlinear dimensionality reduction (NLDR) [31–33] and Statistical hypothesis testing [34, 35] have led to insights on the role of edges and textures [36], color [37], noise [38], lighting [39] and gradients [40] for image datasets.

3 Correlations and power-law Scaling

In this section, we analyze the feature-feature covariance matrix for datasets of varying size, complexity, and origin. We consider real-world as well as synthetic datasets, establish a power-law scaling of their eigenvalues, and relate it to a correlation length.

3.1 Feature-Feature Empirical Covariance Matrix

Let $\{x_a\}_{a=1}^M \subseteq \mathbb{R}^d$ be a set of M data samples composed of d features. We define the data matrix $X_{ai} \in \mathbb{R}^{M \times d}$, constructed of M rows, each corresponding to a single sample. In this work, we focus on the empirical feature-feature covariance matrix, defined as

$$\Sigma_{ij,M} = \frac{1}{M} \sum_{a=1}^M X_{ia} X_{aj} \in \mathbb{R}^{d \times d}. \quad (1)$$

Intuitively, the correlations between the different input features, X_{ia} , should be the leading order characteristic of the dataset. For instance, if the X_{ia} are pixels of an image, we may expect that different pixels will vary similarly across similar images. Conversely, the mean value of an input feature is uninformative, and so we will assume that our data is centered in a pre-processing stage.

A random matrix ensemble is a probability distribution on the set of $d \times d$ matrices that satisfy specific symmetry properties, such as invariance under rotations or unitary transformations. In order to study Eq. (1) using the RMT approach, we define $\Sigma_{ij,a}$ as a single sample realization of the population random matrix ensemble Σ_{ij} , and thus $\Sigma_{ij,M}$ is the empirical ensemble average, i.e. $\Sigma_M = \langle \Sigma_a \rangle_{a \in M} = \frac{1}{M} \sum_{a=1}^M \Sigma_a$ approximating the limits of $M \rightarrow \infty, d \rightarrow \infty$. If M and d are sufficiently large, the statistical properties of Σ_M will be determined entirely by the underlying symmetry of the ensemble.

3.2 Data Exploration

We study the following real-world datasets: MNIST [41], FMNIST [42], CIFAR10 [43], Tiny-IMAGENET [44], and CelebA [45] (downsampled to 109×89 in grayscale). We proceed to center and normalize all the datasets in the pre-processing stage, to remove the uninformative mean contribution. To generate uncorrelated synthetic data, we draw M samples $\{\vec{X}_a \in \mathbb{R}^d, a = 1 \dots M\}$ from a jointly normal distribution $\vec{X}_a \sim \mathcal{N}(0, I_{d \times d})$, and construct the empirical covariance matrix

$\Sigma_M = \frac{1}{M} \sum_{a=1}^M \vec{X}_a \otimes \vec{X}_a \in \mathbb{R}^{d \times d}$. We refer to these datasets as *Synthetic Noise*. To generate correlated synthetic data, we repeat the same process, changing the distribution such that $\vec{X}_a \sim \mathcal{N}(0, \Sigma_{d \times d})$, where we choose a specific form for Σ which produces feature-feature correlations, as

$$\Sigma_{ij}^{\text{Toe}} = \mathbb{1}_{ij} + c|i-j|^\alpha, \quad \alpha, c \in \mathbb{R}. \quad (2)$$

The matrix Σ_{ij}^{Toe} is a full-band Toeplitz matrix. The sign of α dictates whether correlations decay (negative) or intensify (positive) with distance along a one-dimensional feature space¹. We refer to these datasets as *Synthetic Analogues*.

3.3 Correlations Determine the Noise to Data Transition

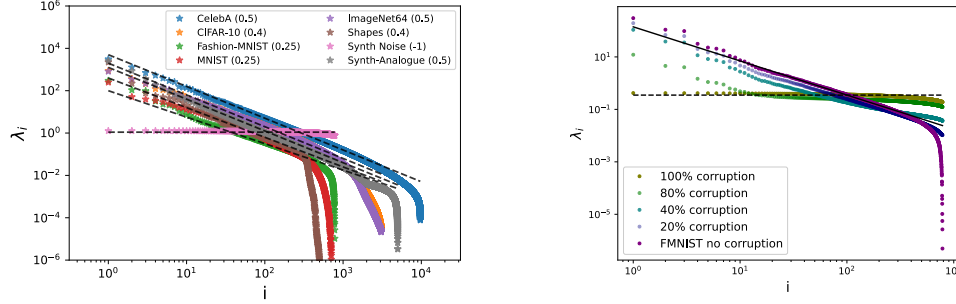


Figure 1: **Left:** Scree plot of $\Sigma_{ij,M}$ for several different vision datasets, as well as for synthetic noise and a synthetic analogue with fixed α . Here, the number of samples is taken to be the entire dataset for each real-world dataset, and $M = 50000$ for the synthetic data, where we set $c = 1$. Different colors indicate different α values, given in the legend. We see a clear scaling law for the eigenvalue bulk as $\lambda_i \propto i^{-1-\alpha}$ where all real-world datasets display $\alpha \leq 1/2$. **Right:** Interpolation of the power-law scaling parameter α value from $\alpha = 1/4$ (purple) to $\alpha = -1$ (green) by corrupting the FMNIST dataset with a varying amount of normally distributed noise.

We begin by reproducing and extending some of the results from Maloney et al. [2]. In Fig. 1, we show the $\Sigma_{ij,M}$ eigenvalue scaling for the different classes of data (*i.e.* real-world, synthetic noise and synthetic analogues). We find that for all datasets, the bulk of the eigenvalues scales as a power-law

$$\lambda_i \propto i^{-1-\alpha}, \quad \alpha \in \mathbb{R}, \quad i = 10, \dots, d_{\text{bulk}}, \quad (3)$$

where $i = 10$ is approximately where the scaling law behavior begins and d_{bulk} is the effective bulk size, where the power-law abruptly terminates. We stress that this behavior repeats across all datasets, regardless of origin and complexity.

The value of α can be readily explained in terms of correlations within our synthetic analogue construction. Taking the Fourier Transform of the second term in Eq. (2), the bulk spectrum is given by Appendix A as

$$\lambda_i^{\text{bulk}} = \frac{c}{2} \sqrt{\frac{2}{\pi}} \sin\left(\frac{\pi\alpha}{2}\right) \Gamma(\alpha+1) |i|^{-1-\alpha}, \quad (4)$$

where $\Gamma(x)$ is the Gamma function. This implies that the value of α determines the strength of correlations in the original data covariance matrix. For real-world data, we consistently find that $\alpha > 0$, which corresponds to increasing correlations between different features. In contrast, for synthetic noise, the value of $\alpha \sim -1$, and the power-law behavior vanishes. Interpolating between synthetic noise, and real-world-data, the synthetic analogue produces a power-law scaling, which can be tuned from $-1 < \alpha \leq 0$, in the case of decaying long range correlations, or $0 \leq \alpha < \infty$ for increasing correlations, to match any real-world dataset we examined. Lastly, we can extend this statement further and verify the transition from correlated to uncorrelated features by corrupting a real-world dataset (FMNIST) and observing the continuous deterioration of the power-law from $\alpha \sim 1/4$ to $\alpha = -1$, implying that the synthetic analogue can mimic the bulk behavior of both clean and corrupted data.

¹Correlation strength which grows with distance is a feature commonly found in some one-dimensional physical systems, such as the Coulomb and Riesz gases [46, 47], which display an inverse power-law repulsion, while decaying correlations are common in the 1-d Ising model [48].

4 Global and Local Statistical Structure

4.1 Random Matrix Theory

In this section, we begin by describing the RMT diagnostic tools, often used to characterize chaotic quantum systems, with which we obtain our main results. We define the matrix ensemble under investigation, then provide an overview of each diagnostic, concluding with a summary of results for the specific matrix ensemble relevant to both real-world and synthetic datasets. While we provide an overview of each diagnostic, we refer the reader to Tao [49], Kim et al. [50] for a more complete review. We then apply these tools to gain insights into the statistical structure of the datasets.

4.1.1 Spectral Density

The empirical spectral density of a matrix Σ is defined as,

$$\rho_{\Sigma}(\lambda) = \frac{1}{n} \sum_{i=1}^n \delta(\lambda - \lambda_i(\Sigma)), \quad (5)$$

where δ is the Dirac delta function, and the $\lambda_i(\Sigma)$, $i = 1, \dots, n$, denote the n eigenvalues of Σ , including multiplicity. The limiting spectral density is defined as the limit of Eq. (5) as $n \rightarrow \infty$.

4.1.2 Level Spacing Distribution and r -statistics

The level spacing distribution measures the probability density for two adjacent eigenvalues to be in the spectral distance s , in units of the mean level spacing Δ . The procedure for normalizing all distances in terms of the local mean level spacing is often referred to as unfolding. We unfold the spectrum of the empirical covariance matrix $\Sigma(\rho)$ by standard methods [50], reviewed in Appendix A. Ultimately, the transformation $\lambda_i \rightarrow e_i = \tilde{\rho}(\lambda_i)$ is performed such that e_i shows an approximately uniform distribution with unit mean level spacing. Once unfolded, the level spacing is given by $s_i = e_{i+1} - e_i$, and its probability density function $p(s)$ is measured.

The level spacing distribution captures information about the short-range spectral correlations, demonstrating the presence of level repulsion, *i.e.*, whether $p(s) \rightarrow 0$ as $s \rightarrow 0$, which is a common trait of RMT ensembles, as the probability of two eigenvalues being exactly degenerate is zero.

The level spacing distribution $p(s)$ for certain systems is known. For integrable systems, it follows the Poisson distribution $p(s) = e^{-s}$, while for chaotic systems, it is given by the Wigner surmise

$$p_{\beta}(s) = Z_{\beta} s^{\beta} e^{-b_{\beta} s^2}, \quad (6)$$

where β , Z_{β} , and b_{β} depend on which universality class of random matrices the covariance matrix belongs to [51]. In this work, we consider matrices that fall under the universality class of the Gaussian Orthogonal Ensemble (GOE), for which $\beta = 1$.

While the level spacing distribution depends on unfolding the eigenspectrum, which is only heuristically defined and has some arbitrariness, it is useful to have additional diagnostics of chaotic behavior that bypass the unfolding procedure. The r -statistics, first introduced in [52], is such a diagnostic tool for short-range correlations, defined without the necessity to unfold the spectrum.

Given the level spacings s_i , defined as the differences between adjacent eigenvalues $\dots < \lambda_i < \lambda_{i+1} < \dots$ without unfolding, one defines the following ratios:

$$r_i = \frac{\text{Min}(s_i, s_{i+1})}{\text{Max}(s_i, s_{i+1})}, \quad 0 \leq r_i \leq 1. \quad (7)$$

The expectation value of the ratios r_i takes very specific values if the energy levels are the eigenvalues of random matrices: for matrices in the GOE the ratio is $\langle r \rangle \approx 0.53590$. The value becomes typically smaller for integrable systems, approaching $\langle r \rangle \approx 0.38629$ for a pure Poisson process [53].

4.1.3 Spectral Form Factor

The spectral form factor (SFF) is a long-range observable that probes the agreement of a given unfolded spectrum with RMT at energy scales much larger than the mean level spacing. It can be used to detect spectral rigidity, which is a signature of quantum chaos.

The SFF is defined as the Fourier transform of the spectral two-point correlation function [54, 55]

$$K(\tau) = |Z(\tau)|^2 / Z(0)^2 \simeq \frac{1}{Z} \mathbb{E} \left\langle \left| \sum_i \rho(e_i) e^{-i2\pi e_i \tau} \right|^2 \right\rangle, \quad (8)$$

where $Z(\tau) = \text{Tr} e^{-i\tau \Sigma(\rho_\Sigma)}$. The second equality is the numerically evaluated SFF [56], where e_i is the unfolded spectrum, and $Z = \sum_i |\rho(e_i)|^2$ is chosen to ensure that $\lim_{\tau \rightarrow \infty} K(\tau) \approx 1$.

The SFF has been computed analytically for the GOE, and it reads

$$K_{\text{GOE}}(\tau) = 2\tau - \tau \ln(1 + 2\tau) \text{ for } 0 < \tau < 1, \quad K_{\text{GOE}}(\tau) = 1 \text{ for } 1 \leq \tau. \quad (9)$$

Several universal features occur in chaotic RMT ensembles, manifesting in Eq. (9) and discussed in detail in Liu [55], Kim et al. [50]. We mention here only two: (i) The constancy of $K(\tau)$ for $\tau \geq 1$ is simply a consequence of the discreteness of the spectrum. (ii) The existence of a timescale that characterizes the ergodicity of a dynamical system. It is defined as the time when the SFF of the dynamical system converges to the universal RMT computation. More concretely, it is indicated by the onset of the universal linear ramp as in (9), which is absent in non-ergodic systems.

4.2 Insights from the Global and Local Statistical Structure

4.2.1 Eigenvalues Distributions

While the scaling behavior of the bulk of eigenvalues is certainly meaningful, it is not the only piece of information that can be extracted from the empirical covariance matrix. Particularly, it is natural to inquire whether the origin of the power-law scaling determines also the degeneracy of each eigenvalue. We can test this hypothesis by comparing the global and local statistics of the bulk between real-world data and their synthetic analogue counterparts.

For the synthetic datasets we generate, there are known predictions for the spectral density, level spacing distribution, r -statistics and spectral form factor. In these special cases, the empirical covariance matrix in Eq. (1) is known as a Wishart matrix [57]: $\Sigma_{ij,M} \sim \mathcal{W}_d(\Sigma, M)$.

For a Wishart matrix, the spectral density $\rho(\lambda)$ is given by the generalized Marčenko-Pastur (MP) law [22], which depends on the details of Σ and given in Appendix B. For $\Sigma = \sigma^2 I_d$, the spectral density is given explicitly by the MP distribution as

$$\rho(\lambda) = \frac{1}{2\pi\sigma^2} \frac{\sqrt{(\lambda_{\max} - \lambda)(\lambda - \lambda_{\min})}}{\gamma\lambda} \quad \text{for } \lambda \in [\lambda_{\min}, \lambda_{\max}] \text{ and } 0 \text{ otherwise}, \quad (10)$$

where $\lambda_{\max/\min} = \sigma^2(1 \pm \sqrt{\gamma})^2$, $\gamma \equiv d/M$ and $d, M \rightarrow \infty$.

In Fig. 2, we show that the synthetic analogues capture not only the scaling behavior of the eigenvalue bulk, but also the spectral density and the distribution of eigenvalues, for ImageNet, CIFAR10, and FMNIST, measured by the Kullback–Leibler divergence (KL) [58]. We further emphasize this point by contrasting the distributions with the MP distribution, which accurately captures the spectral density of the synthetic noise datasets. This measurement alone is not sufficient to determine that the system is well approximated by RMT, and we must study several other statistical diagnostics.

4.2.2 Level Spacing Diagnostics

RMT predicts that certain local and global statistical properties are determined uniquely by symmetry. Therefore, the empirical covariance matrix must lie either in the GOE ensemble if it is akin to a quantum chaotic system² or in the Poisson ensemble, if it corresponds to an integrable system.

Both the level spacing and r statistics (the ratio of adjacent level spacings) probability distribution functions for a Wishart matrix in the limit of $d, M \rightarrow \infty$ and $d/M = \gamma$, are given by the GOE universality class:

$$p_{\text{GOE}}(s) = \frac{\pi}{2} s e^{-\frac{\pi}{4}s^2}, \quad p_{\text{GOE}}(r) = \frac{16}{27} \frac{(r + r^2)}{(1 + r + r^2)^{5/2}} \Theta(1 - r), \quad \langle r \rangle_{\text{GOE}} = 4 - 2\sqrt{3}, \quad (11)$$

while the SFF is given by Eq. (9).

²Large random real symmetric matrices belong in the orthogonally invariant class.

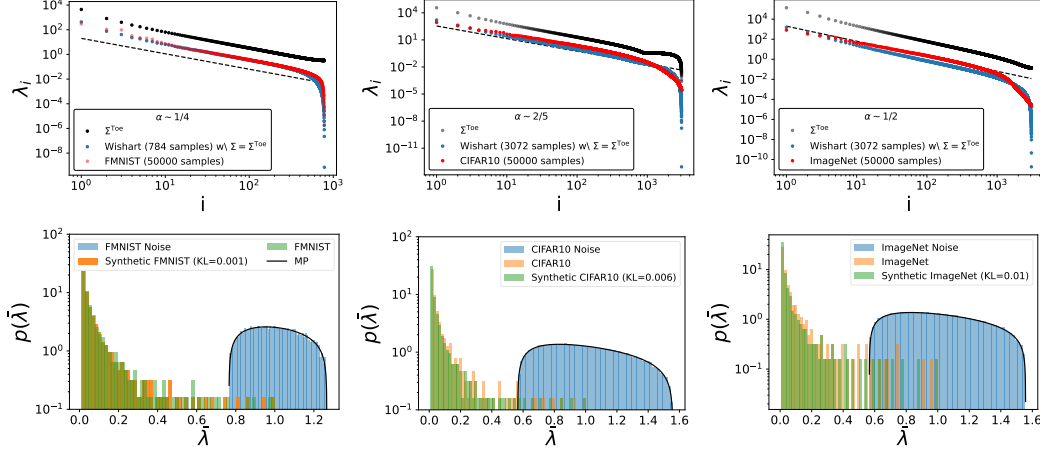


Figure 2: **Top row:** Scree plot of $\Sigma_{ij,M}$ for several different configurations and datasets. We show the eigenvalues of the population covariance matrix Σ^{Toe} , the eigenvalues of the empirical covariance using the same Σ^{Toe} , with $M = d$, and finally the eigenvalues for the empirical covariance of the full real-world dataset with $M = 50000$. The datasets used here are (left to right): FMNIST, CIFAR10, ImageNet. **Bottom row:** Spectral density for the bulk of eigenvalues for the same datasets, as well as a comparison against synthetic noise of the same dimensions. The $\bar{\lambda}$ indicates normalization over the maximal eigenvalue among the bulk. We also provide the KL divergence between the synthetic analogues and the real-world data distributions.

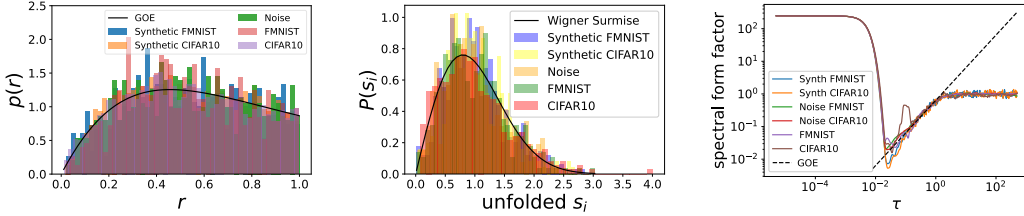


Figure 3: The r probability density (**left**), the unfolded level spacing distribution (**center**) and the spectral form factor (**right**) of Σ_M for FMNIST, CIFAR10, their synthetic analogues, and synthetic noise, obtained with $M = 50000$. Black curves indicate the RMT predictions for the GOE distribution from Eq. (11). These results indicate that the bulk of real-world data eigenvalues belongs to the GOE universality class, and that system has enough statistics to converge to the RMT predictions.

In Fig. 3, we demonstrate that the bulk of eigenvalues for various real-world datasets behaves as the energy eigenvalues of a quantum chaotic system described by the GOE universality class. This result is matched by both the synthetic noise and the synthetic analogues, as is expected of a Wishart matrix. Here, the dataset size is taken to be $M = 50000$ samples, and the results show that this sample size is sufficient to provide a proper sampling of the underlying ensemble.

4.2.3 Effective Convergence

Having confirmed that synthetic analogues provide a good proxy for the bulk structure for a large fixed dataset size, we may now ask how the statistical results depend on the number of samples.

As discussed in Section 3.1, Σ_M can be interpreted as an ensemble average over single realizations of the true population covariance matrix Σ . As the number of realizations M increases, a threshold value of M_{crit} is expected to appear when the space of matrices that matches the effective dimension of the true population matrix is fully explored.

The specific value of M_{crit} can be approximated without knowing the true effective dimension by considering two different evaluation metrics. Firstly, convergence of the local statistics of Σ_M , given by the point at which its level spacing distribution and r value approximately match their respective RMT ensemble expectations. Secondly, convergence of the global spectral statistics, both of Σ_M to that of Σ and of the empirical parameter α_M to its population expectation α .

Here, we define these metrics and measure them for different datasets, obtaining analytical expectations for the synthetic analogues, which accurately mimic their real-world counterparts.

We can deduce M_{crit} from the local statistics by measuring the difference between the empirical average r value and the theoretical one given by

$$|r_M - r_{\text{RMT}}| = \delta(M)r_{\text{RMT}}, \quad (12)$$

where r_{RMT} is known for the GOE to be $r_{\text{GOE}} = 4 - 2\sqrt{3} \simeq 0.5359$ and $r_{\text{PE}} \simeq 0.3863$ for the Poisson ensemble.

Next, we compare the results obtained for M_{crit} from $\delta(M)$ to the one obtained from the global statistics by using a spectral distance measure for the eigenvalue bulk given by

$$|\alpha_M - \alpha| = \Delta(M), \quad (13)$$

where α_M is the measured value obtained by fitting a power-law to the bulk of eigenvalues for a fixed dataset size M , while α represents the convergent value including all samples from a dataset.

Lastly, we compare the full empirical covariance matrix with the convergent result obtained using the full dataset by taking

$$|\Sigma_M - \Sigma| = \epsilon(M)|\Sigma|, \quad (14)$$

where $|A|$ is the spectral norm of A , and $\epsilon(M)$ will be our measure of the distance between the two covariance matrices.

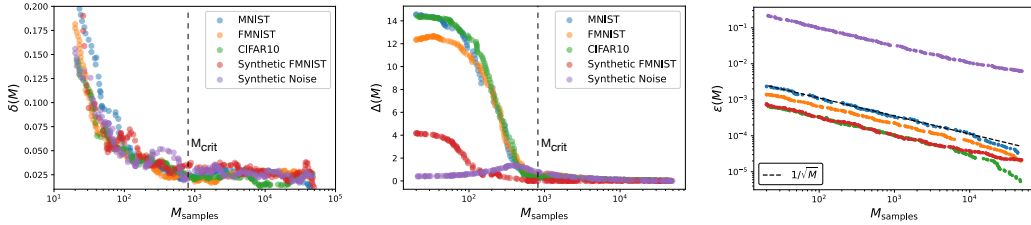


Figure 4: **Left:** The r distance metric $\delta(M)$ for the bulk of eigenvalues. **Center:** The α distance metric $\Delta(M)$ for the bulk of eigenvalues. **Right:** The full matrix comparison metric $\epsilon(M)$. We show the results for CIFAR10, FMNIST, synthetic noise, and the FMNIST synthetic analogue as a function of the number of samples. The results show that the bulk distances decrease as $1/M$, where M is the number of samples, asymptoting to a constant value at similar values of $M_{\text{crit}} \sim d$ (black dashed), where d is the number of features.

In Fig. 4, we show the results for each of these metrics separately as a function of the number of samples M . We find that the $\delta(M)$ parameter, which is a measure of local statistics, converges to the expected GOE value at roughly the same M_{crit} as the entirely independent $\Delta(M)$ parameter, which measures the scaling exponent α . The combination of these two metrics confirms empirically that the system has become ergodic at sample sizes roughly $M_{\text{crit}} \sim d$, which is much smaller than the typical size of the datasets.

4.2.4 Datasets Entropy

The Shannon entropy [59] of a random variable a measure of information, inherent to the variable's possible outcomes [60], given by $H = -\sum_{i=1}^n p_i \log(p_i)$ where p_i is the probability of a given outcome and n is the number of possible states. For covariance matrices, we define p_i given the spectrum as $p_i = \lambda_i / \sum_{i=1}^{n_{\text{bulk}}} \lambda_i$, where n_{bulk} is the number of bulk eigenvalues.

In Fig. 5 (left) we plot the Shannon entropies of real and synthetic datasets as a function of the number of samples. The entropies grow linearly and reach a plateau whose value is related to the correlation strength, with strong correlation corresponding to low entropy. We see the same entropy for both the synthetic and real datasets that have the same scaling exponent, implying that they also share the same eigenvalues degeneracy.

²We omit synthetic noise from the center panel, as $\alpha = -1$ regardless of M .

4.2.5 Entropy, Scaling and r-Statistics

In Fig. 5 (left), we see that the entropy saturation is correlated with the effective convergence in Fig. 4 as a function of the number of samples, while the middle and right plots show the correlation between the convergence of the entropy, the scaling exponent and the r-statistics, respectively. We see that real data and synthetic data with the same scaling exponent exhibit similar convergence behaviour.

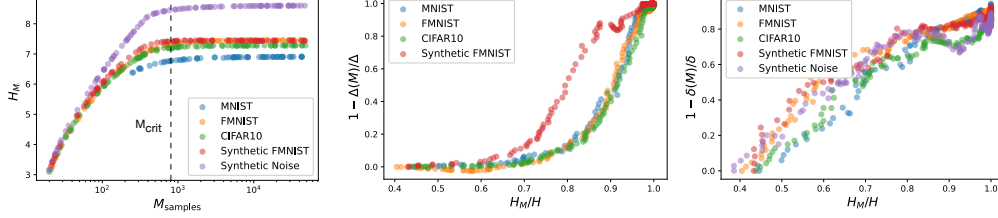


Figure 5: Convergence of the various metrics in Eqs. (12) to (14) in relation to entropy for the bulk of eigenvalues. **Left:** The Shannon entropy H_M as a function of the dataset size M . **Center:** Convergence of the normalized α metric $1 - \Delta_M/\Delta$ to its asymptotic value as a function of the normalized entropy H_M/H . **Right:** Convergence of the normalized r statistics metric $1 - \delta_M/\delta$ to its asymptotic value as a function of the normalized entropy H_M/H . We show the results for CIFAR10, FMNIST, MNIST, synthetic noise, and the FMNIST synthetic analogue⁴.

5 Conclusions

In this paper, we have presented fundamental results regarding the universal structure of real-world and synthetic datasets. Our findings indicate that these datasets exhibit scaling laws, and the distribution of eigenvalues predominantly aligns with the GOE universality class of RMT.

While our empirical results indicate that real-world data displays chaotic properties, the exact source is not evident. We believe that further work is necessary to determine whether it is due to the underlying strongly correlated structure that is manifest in real-world data, or if it stems from the chaotic sampling process that generates noise, which is captured in the finer details encoded in the eigenvalue bulk.

Our approach, based on synthetic analogues to real-world data, lays the groundwork for considering neural scaling laws at the distribution level, capturing higher moments and eigenvalue distributions beyond mean scaling factors. This comprehensive perspective provides deeper insights into the underlying dynamics. With these observations in hand, we can further enhance our understanding of these scaling laws and their connections to fundamental principles.

Though primarily focused on image datasets, extending research to language datasets offers valuable insights into the universality of scaling laws across modalities. Additionally, the interplay between eigenvectors and eigenvalues in neural networks merits further exploration, as both components likely play crucial roles in the way neural networks process information. Studying the generation of synthetic eigenvectors and eigenvalues from RMT ensembles provides avenues to understand network behavior and dynamics.

Practically, our study reveals the range of real scalings observed when examining different α values for corrupted and uncorrupted data, enhancing our knowledge of model vulnerabilities and robustness against adversarial perturbations. Furthermore, our work introduces a novel approach to assess the fidelity and perceptual quality of artificially-generated images through scaling analysis, contributing to the evaluation of generative model qualities.

In summary, we have presented original results on the underlying scaling laws appearing in datasets and their implications, extending beyond traditional scaling factors to encompass more general statistical properties and the distribution of eigenvalues. The exploration of language data and extension of neural scaling laws, understanding the chaotic nature of the sampling processes, and the relationship between eigenvectors and eigenvalues via RMT represents exciting avenues for future research. Additionally, our findings have practical applications in the context of adversarial attacks and the evaluation of artificially-generated images. By advancing our understanding in these areas, we can enhance the robustness, interpretability, and performance of neural networks across domains.

⁴We omit synthetic noise from the center panel, as $\alpha = -1$ regardless of M .

6 Acknowledgements

We would like to thank Yohai Bar-Sinai, Marat Freytsis, Alex Maloney, Dan Roberts, and Jamie Sully for useful discussions and comments. N.L. would like to thank the Milner Foundation for the award of a Milner Fellowship. The work of Y.O. is supported in part by Israel Science Foundation Center of Excellence. This work was performed in part at Aspen Center for Physics, which is supported by the U.S. National Science Foundation grant PHY-2210452.

References

- [1] Jared Kaplan, Sam McCandlish, Tom Henighan, Tom B. Brown, Benjamin Chess, Rewon Child, Scott Gray, Alec Radford, Jeffrey Wu, and Dario Amodei. Scaling laws for neural language models, 2020.
- [2] Alexander Maloney, Daniel A. Roberts, and James Sully. A solvable model of neural scaling laws, 2022.
- [3] Thomas Guhr, Axel Müller-Groeling, and Hans A. Weidenmüller. Random-matrix theories in quantum physics: common concepts. *Physics Reports*, 299(4-6):189–425, jun 1998. doi: 10.1016/s0370-1573(97)00088-4. URL <https://doi.org/10.1016%2Fs0370-1573%2897%2900088-4>.
- [4] O. Bohigas, M. J. Giannoni, and C. Schmit. Characterization of chaotic quantum spectra and universality of level fluctuation laws. *Physical review letters*, 52(1):1, 1984.
- [5] M. L. Mehta. *Random matrices*, volume 111. Academic Press, 1991.
- [6] A. Pandey. Random matrix theory and quantum chaos. *Reviews of Modern Physics*, 55(4):807–823, 1983.
- [7] V. Plerou, P. Gopikrishnan, B. Rosenow, L. A. N. Amaral, H. E. Stanley, and Stanley M. S. Random matrix theory and financial markets. *Physical Review E*, 60(5):6519–6532, 1999.
- [8] T. A. Brody. Random matrix models in nuclear physics. *Reports on Progress in Physics*, 44(4):1125–1191, 1981.
- [9] K. B. Efetov. *Supersymmetry and disorder in quantum mechanics*. Cambridge University Press, 1997.
- [10] Robert M. Gray. Toeplitz and circulant matrices: A review. *Foundations and Trends® in Communications and Information Theory*, 2(3):155–239, 2006. ISSN 1567-2190. doi: 10.1561/0100000006. URL <http://dx.doi.org/10.1561/0100000006>.
- [11] Danny Hernandez, Tom Brown, Tom Conerly, Nova DasSarma, Dawn Drain, Sheer El-Showk, Nelson Elhage, Zac Hatfield-Dodds, Tom Henighan, Tristan Hume, Scott Johnston, Ben Mann, Chris Olah, Catherine Olsson, Dario Amodei, Nicholas Joseph, Jared Kaplan, and Sam McCandlish. Scaling laws and interpretability of learning from repeated data, 2022.
- [12] Maor Ivgi, Yair Carmon, and Jonathan Berant. Scaling laws under the microscope: Predicting transformer performance from small scale experiments. In Yoav Goldberg, Zornitsa Kozareva, and Yue Zhang, editors, *Findings of the Association for Computational Linguistics: EMNLP 2022, Abu Dhabi, United Arab Emirates, December 7-11, 2022*, pages 7354–7371. Association for Computational Linguistics, 2022. URL <https://aclanthology.org/2022.findings-emnlp.544>.
- [13] Ibrahim M. Alabdulmohsin, Behnam Neyshabur, and Xiaohua Zhai. Re-visiting neural scaling laws in language and vision. In *NeurIPS*, 2022. URL http://papers.nips.cc/paper_files/paper/2022/hash/8c22e5e918198702765ecff4b20d0a90-Abstract-Conference.html.
- [14] Utkarsh Sharma and Jared Kaplan. Scaling laws from the data manifold dimension. *J. Mach. Learn. Res.*, 23:9:1–9:34, 2022. URL <http://jmlr.org/papers/v23/20-1111.html>.

- [15] Ben Sorscher, Robert Geirhos, Shashank Shekhar, Surya Ganguli, and Ari Morcos. Beyond neural scaling laws: beating power law scaling via data pruning. In *NeurIPS*, 2022. URL http://papers.nips.cc/paper_files/paper/2022/hash/7b75da9b61eda40fa35453ee5d077df6-Abstract-Conference.html.
- [16] Lukasz Debowski. A simplistic model of neural scaling laws: Multiperiodic santa fe processes. *CoRR*, abs/2302.09049, 2023. doi: 10.48550/arXiv.2302.09049. URL <https://doi.org/10.48550/arXiv.2302.09049>.
- [17] Patrick Fernandes, Behrooz Ghorbani, Xavier Garcia, Markus Freitag, and Orhan Firat. Scaling laws for multilingual neural machine translation. *CoRR*, abs/2302.09650, 2023. doi: 10.48550/arXiv.2302.09650. URL <https://doi.org/10.48550/arXiv.2302.09650>.
- [18] Jeffrey Pennington and Pratik Worah. Nonlinear random matrix theory for deep learning. In *Advances in Neural Information Processing Systems*, pages 2637–2646, 2017. URL <https://papers.nips.cc/paper/6857-nonlinear-random-matrix-theory-for-deep-learning>.
- [19] Zhenyu Liao, Romain Couillet, and Michael W Mahoney. A random matrix analysis of random fourier features: beyond the gaussian kernel, a precise phase transition, and the corresponding double descent. *Journal of Statistical Mechanics: Theory and Experiment*, 2021(12):124006, dec 2021. doi: 10.1088/1742-5468/ac3a77.
- [20] Zhenyu Liao and Michael W. Mahoney. Hessian eigenspectra of more realistic nonlinear models, 2021.
- [21] Charles H Martin and Michael W Mahoney. Traditional and heavy-tailed self-regularization in neural network models. *arXiv preprint arXiv:1901.08276*, 2019. URL <https://arxiv.org/abs/1901.08276>.
- [22] Romain Couillet and Zhenyu Liao. *Random Matrix Methods for Machine Learning*. Cambridge University Press, 2022. doi: 10.1017/9781009128490.
- [23] Midjourney. Midjourney, 2022. URL <https://www.midjourney.com/>.
- [24] Robin Rombach, Andreas Blattmann, Dominik Lorenz, Patrick Esser, and Björn Ommer. High-resolution image synthesis with latent diffusion models, 2021.
- [25] Momina Masood, Marriam Nawaz, Khalid Mahmood Malik, Ali Javed, and Aun Irtaza. Deep-fakes generation and detection: State-of-the-art, open challenges, countermeasures, and way forward, 2021.
- [26] Ian J. Goodfellow, Jonathon Shlens, and Christian Szegedy. Explaining and harnessing adversarial examples, 2015.
- [27] Nicholas Carlini and David Wagner. Towards evaluating the robustness of neural networks, 2017.
- [28] Rimsha Rafique, Rahma Gantassi, Rashid Amin, Jaroslav Frnda, Aida Mustapha, and Asma Hassan Alshehri. Deep fake detection and classification using error-level analysis and deep learning. *Scientific Reports*, 13(1):7422, 2023. doi: 10.1038/s41598-023-34629-3. URL <https://doi.org/10.1038/s41598-023-34629-3>.
- [29] Karl Pearson. Liii. on lines and planes of closest fit to systems of points in space. *Philosophical Magazine*, 2(11):559–572, 1901. doi: 10.1080/14786440109462720.
- [30] Ian Jolliffe. *Principal Component Analysis*. John Wiley & Sons, Ltd, 2005. ISBN 9780470013199. doi: <https://doi.org/10.1002/0470013192.bsa501>. URL <https://onlinelibrary.wiley.com/doi/abs/10.1002/0470013192.bsa501>.
- [31] Katherine C. Kempfert, Yishi Wang, Cuixian Chen, and Samuel W. K. Wong. A comparison study on nonlinear dimension reduction methods with kernel variations: Visualization, optimization and classification, 2019.

- [32] Suchismita Das and Nikhil R. Pal. Nonlinear dimensionality reduction for data visualization: An unsupervised fuzzy rule-based approach. *IEEE Transactions on Fuzzy Systems*, 30(7): 2157–2169, jul 2022. doi: 10.1109/tfuzz.2021.3076583. URL <https://doi.org/10.1109/2Ftfuzz.2021.3076583>.
- [33] Shaeela Ayesha, Muhammad Kashif Hanif, and Ramzan Talib. Overview and comparative study of dimensionality reduction techniques for high dimensional data. *Information Fusion*, 59:44–58, 2020. ISSN 1566-2535. doi: <https://doi.org/10.1016/j.inffus.2020.01.005>. URL <https://www.sciencedirect.com/science/article/pii/S156625351930377X>.
- [34] R Nuzzo. Statistical errors: P values, the ‘gold standard’ of statistical validity, are not as reliable as many scientists assume. *Nature*, 506(7487):150–152, 2014. doi: 10.1038/506150a. URL <https://doi.org/10.1038/506150a>.
- [35] Hanxiang Hao, Emily R Bartusiak, David Guera, Daniel Mas Montserrat, Sriram Baireddy, Ziyue Xiang, Sri Kalyan Yarlagadda, Ruiting Shao, Janos Horvath, Justin Yang, Fengqing Zhu, and Edward J Delp. Deepfake detection using multiple data modalities. *IEEE Transactions on Information Forensics and Security*, 17(11):2873–2886, 2022. doi: 10.1109/TIFS.2022.3188046.
- [36] Patchara Sutthiwan, Yun Q. Shi, Wei Su, and Tian-Tsong Ng. Rake transform and edge statistics for image forgery detection. In *2010 IEEE International Conference on Multimedia and Expo*, pages 1463–1468, 2010. doi: 10.1109/ICME.2010.5583264.
- [37] Yanyang Yan, Wenqi Ren, and Xiaochun Cao. Recolored image detection via a deep discriminative model. *IEEE Transactions on Information Forensics and Security*, 14(1):5–17, 2019. doi: 10.1109/TIFS.2018.2834155.
- [38] Zongsheng Yue, Hongwei Yong, Qian Zhao, Lei Zhang, and Deyu Meng. Variational denoising network: Toward blind noise modeling and removal, 2020.
- [39] Ron O. Dror, Alan S. Willsky, and Edward H. Adelson. Statistical characterization of real-world illumination. *Journal of vision*, 4 9:821–37, 2004.
- [40] Maria Zontak and Michal Irani. Internal statistics of a single natural image. In *CVPR 2011*, pages 977–984, 2011. doi: 10.1109/CVPR.2011.5995401.
- [41] Yann LeCun, Léon Bottou, Yoshua Bengio, and Pierre Haffner. The mnist database of handwritten digits. <http://yann.lecun.com/exdb/mnist/>, 2010.
- [42] Han Xiao, Salim Rasul, and Richard S Zemel. Fashion-mnist: a novel image classification benchmark based on fashion articles. *arXiv preprint arXiv:1708.07747*, 2017.
- [43] Cifar-10. URL <https://www.cs.toronto.edu/~kriz/cifar.html>.
- [44] Antonio Torralba, Andreas A Efros, and Christopher Anderson. Tiny imagenet: A benchmark for evaluation of image classification algorithms. *International Journal of Computer Vision*, 69 (2):203–228, 2008.
- [45] Ziwei Liu, Zihang Luo, Xiaogang Wang, and Xiaoou Tang. Celeba: A large-scale celebrity face attribute dataset. <http://mmlab.ie.cuhk.edu.hk/projects/CelebA.html>, 2015.
- [46] T. D. Lee and C. N. Yang. Statistical mechanics of charged particles. *Zeitschrift für Physik*, 196:433–453, 1966. doi: 10.1007/BF02750405.
- [47] M. A. Smorodinsky. On the classical motion of charged particles. *Journal of Mathematical Physics*, 4:1005–1011, 1953. doi: 10.1063/1.1703719.
- [48] Ernst Ising. Beitrag zur theorie des ferromagnetismus. *Zeitschrift für Physik*, 31:853–865, 1925. doi: 10.1007/BF01343133.
- [49] Terence Tao. *Topics in random matrix theory*, volume 132. American Mathematical Soc., 2012.

- [50] Joonho Kim, Yaron Oz, and Dario Rosa. Quantum chaos and circuit parameter optimization. *Journal of Statistical Mechanics: Theory and Experiment*, 2023(2):023104, feb 2023. doi: 10.1088/1742-5468/acb52d. URL <https://doi.org/10.1088/1742-5468/acb52d>.
- [51] M. L. Mehta. *Random Matrices*. 3 edition, 2004.
- [52] Vadim Oganessian and David A. Huse. Localization of interacting fermions at high temperature. *Phys. Rev. B*, 75:155111, 2007. doi: 10.1103/PhysRevB.75.155111. URL <https://link.aps.org/doi/10.1103/PhysRevB.75.155111>.
- [53] Y. Y. Atas, E. Bogomolny, O. Giraud, and G. Roux. Distribution of the ratio of consecutive level spacings in random matrix ensembles. *Phys. Rev. Lett.*, 110:084101, 2013. doi: 10.1103/PhysRevLett.110.084101. URL <https://link.aps.org/doi/10.1103/PhysRevLett.110.084101>.
- [54] Jordan S. Cotler, Guy Gur-Ari, Masanori Hanada, Joseph Polchinski, Phil Saad, Stephen H. Shenker, Douglas Stanford, Alexandre Streicher, and Masaki Tezuka. Black holes and random matrices. *J. High Energy Phys.*, 2017:118, 2017. doi: 10.1007/JHEP05(2017)118. URL [https://link.springer.com/article/10.1007/JHEP05\(2017\)118](https://link.springer.com/article/10.1007/JHEP05(2017)118).
- [55] Junyu Liu. Spectral form factors and late time quantum chaos. *Physical Review D*, 98(8), oct 2018. doi: 10.1103/physrevd.98.086026. URL <https://doi.org/10.1103/physrevd.98.086026>.
- [56] J. Juntajs, J. Bonca, T. Prosen, and L. Vidmar. Quantum chaos challenges many-body localization. *Phys. Rev. E*, 102:062144, 2020. doi: 10.1103/PhysRevE.102.062144. URL <https://link.aps.org/doi/10.1103/PhysRevE.102.062144>.
- [57] John Wishart. Generalised product moment distribution in samples from an indefinitely large population. *Biometrika*, 20(1-2):30–52, 1928.
- [58] Solomon Kullback and Richard A Leibler. Information theory and statistics. *The Annals of Mathematical Statistics*, 22(1):79–86, 1951.
- [59] Claude Elwood Shannon. A mathematical theory of communication. *Bell System Technical Journal*, 27(3):379–423, 1948.
- [60] Alfred Rényi. On measures of information and entropy. *Proceedings of the Fourth Berkeley Symposium on Mathematical Statistics and Probability*, 1(4):547–561, 1956.
- [61] Jack W Silverstein and Z. D. Bai. On the empirical distribution of eigenvalues of a class of large dimensional random matrices. *Journal of Multivariate Analysis*, 54(2):175–199, 1995.

A The Unfolding Procedure

Here, we provide additional details on the unfolding procedure used to produce Fig. 3 in the main text.

Care must be taken when analyzing the eigenvalues of the empirical covariance matrix Σ_M , since they exhibit unavoidable numerical errors. To control for the effect of numerical errors, we adopted a robust phenomenological procedure that utilizes the fact that all eigenvalues of Σ_M must be non-vanishing by definition. To ensure we consider only eigenvalues of Σ_M unimpacted by edge effects, we inspect only the bulk spectrum.

Restricting to the bulk removes many eigenvalues of Σ_M as many are zero for small M . However, for larger M when Σ_M 's structure is clearly visible, this is not the case. The procedure ensures the eigenvalues kept are robust and not significantly impacted by numerical precision. From the significant eigenvalues of the empirical covariance matrix Σ_M , we compute the spectrum λ_i .

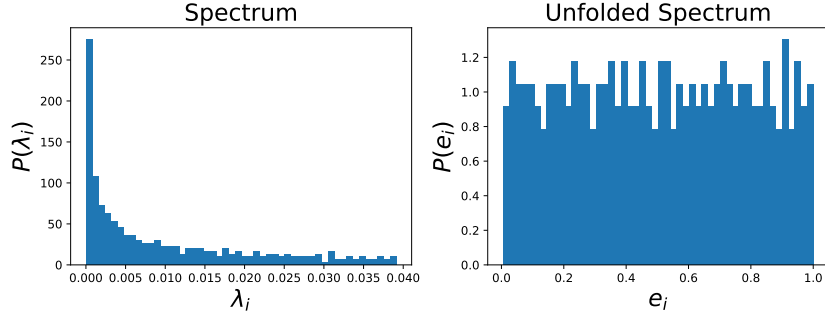


Figure 6: Bulk eigenvalue distribution for the empirical covariance matrix constructed from $M = 50000$ samples of FMNIST, before unfolding (**left**), and after unfolding (**right**). The unfolded spectrum displays approximately unit mean, and is defined on the interval $[0, 1]$.

The unfolding procedure used to derive the unfolded spectrum is as follows:

1. Arrange the non-degenerate eigenvalues, λ_i , of the empirical covariance matrix (Σ_M) in ascending order.
2. Compute the staircase function $S(\lambda)$ that enumerates all eigenstates of the empirical covariance matrix (Σ_M) whose eigenvalues are smaller than or equal to λ .
3. Fit a smooth curve, denoted by $\tilde{\rho}(\lambda)$, to the staircase function. Specifically, we used a 12th-order polynomial as the smooth approximation.
4. Rescale the eigenvalues λ_i as follows:

$$\lambda_i \rightarrow e_i = \tilde{\rho}(\lambda_i) \quad (15)$$

5. By construction, the unfolded eigenvalues e_i should show an approximately uniform distribution with mean level spacing 1. This can be used to check if the procedure was successful by plotting the unfolded levels and checking the flatness of the distribution.

In Fig. 6, we show an example of the unfolding procedure for the FMNIST dataset. Specifically, we show the eigenvalue distribution before ($P(\lambda_i)$) and after ($P(e_i)$) unfolding. Up to the quality of the smoothing function $\tilde{\rho}(\lambda_i)$, the unfolded eigenvalue distribution displays a uniform distribution on the unit interval.

B Spectral Density for Wishart Matrices with a Correlated Features

For $z \in \mathbb{C} \setminus \text{supp}(\rho_\Sigma)$, the Stieltjes transform G and inverse Stieltjes transform ρ_Σ are defined as

$$G(z) = \int \frac{\rho_\Sigma(t)}{z - t} dt = -\frac{1}{n} \mathbb{E} [\text{Tr}(\Sigma - zI_n)^{-1}], \quad \rho_\Sigma(\lambda) = -\frac{1}{\pi} \lim_{\epsilon \rightarrow 0^+} \text{Im} G(\lambda + i\epsilon), \quad (16)$$

where $\mathbb{E}[\dots]$ is taken with respect to the random variable X and $(\Sigma - zI_n)^{-1}$ is the resolvent of Σ .

For the construction, discussed in the main text, and general α , there is no closed form for the spectral density. However, in certain limits, analytical expressions can be derived from the Stieljes transform using Eq. (16). Specifically, given a deterministic expression for Σ , the spectral density can be derived by evoking Theorem 2.6 found in Couillet and Liao [22], which uses the following result by Silverstein and Bai [61]

$$G(z) = \frac{1}{\gamma} \tilde{G}(z) + \frac{1-\gamma}{\gamma z}, \quad \tilde{G}(z) = \left(-z + \frac{1}{M} \text{Tr} \left[\Sigma (I_d + \tilde{G}(z) \Sigma)^{-1} \right] \right)^{-1}, \quad (17)$$

where $\gamma \equiv d/M$ and $d, M \rightarrow \infty$, and we substitute C from the original theorem with Σ .

The empirical covariance matrix of the synthetic analogues discussed in the main text, is a Wishart matrix with a deterministic covariance, and thus fits the requirements of Theorem 2.6, where $\Sigma = \Sigma_{i,j}^{\text{Toe}} = \mathbb{1}_{ij} + c|i-j|^\alpha$. In order to use Eq. (17), it is useful to first diagonalize $\Sigma_{i,j}^{\text{Toe}}$. This can be done by using the discrete Laplace transform (extension of the Fourier transform), leading to

$$\tilde{\Sigma}^{\text{Toe}}(s) = 1 + c \text{Li}_{-\alpha} \left(e^{-\frac{s}{d}} \right) - c e^{-s} \Phi \left(e^{-\frac{s}{d}}, -\alpha, d \right), \quad (18)$$

where $s = 1 \dots d$, $\Phi(x, k, a)$ is the Lerch transcendent, and $\text{Li}(x)$ is the Poly-log function. Because the identity matrix commutes with Σ , we may substitute Eq. (18) in Eq. (17) to obtain

$$\tilde{G}(z) = \frac{1}{-z + \frac{\gamma}{d} S_d(\alpha)}, \quad (19)$$

where we define the sum $S_d(\alpha)$ to be

$$S_d(\alpha) = \sum_{s=1}^d \frac{\tilde{\Sigma}^{\text{Toe}}(s)}{1 + \tilde{G}(z) \tilde{\Sigma}^{\text{Toe}}(s)}. \quad (20)$$

Since the behavior of $\tilde{\Sigma}^{\text{Toe}}(s)$ is intrinsically different for positive and very negative α , we separate the two cases. First, consider the case of $\alpha < -1$, where correlations decay very quickly. In this scenario, the covariance matrix reduces to $\tilde{\Sigma}^{\text{Toe}}(s) \simeq 1$.

Here, $S_d(\alpha)$ is given simply by the $\alpha \rightarrow \infty$ limit

$$S_d(\alpha \rightarrow -\infty) = \sum_{k=1}^d \frac{1}{1 + \tilde{G}(z)} = \frac{d}{1 + \tilde{G}(z)}, \quad (21)$$

which is precisely the case of $\Sigma = I_d$.

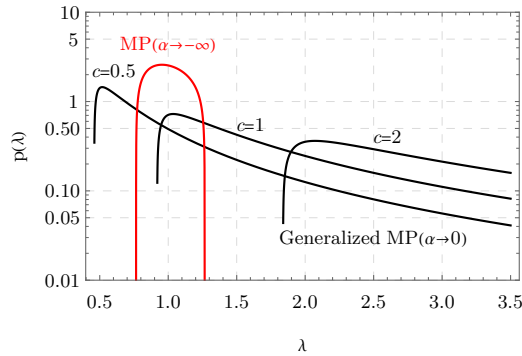


Figure 7: Theoretical predictions for the spectral density of a Wishart matrix. **Black** curves represent the generalized MP distribution, given by the solution to the inverse Stieljes transform in Eq. (28), the **red** curve is the MP distribution. The black curves have a value of $c = 0.5, 1, 2$ going from left to right, and $\gamma = 784/50000$ for all curves.

Solving Eq. (19) using the above result yields the following expression for $\tilde{G}(z)$

$$\tilde{G}(z) = \frac{-1 - z + \gamma - \sqrt{(-1 - z + \gamma)^2 - 4z}}{2z}. \quad (22)$$

Finally, substituting Eq. (22) into Eq. (16) leads to the known Marčenko-Pastur (MP) law [22]

$$\rho(\lambda) = \frac{1}{2\pi} \frac{\sqrt{(\lambda_{\max} - \lambda)(\lambda - \lambda_{\min})}}{\gamma\lambda} \quad \text{for } \lambda \in [\lambda_{\min}, \lambda_{\max}] \text{ and 0 otherwise,} \quad (23)$$

where $\lambda_{\max/\min} = (1 \pm \sqrt{\gamma})^2$.

The other interesting limit is that of $\alpha > -1$, in which the correlations do not decay quickly, and for $d \rightarrow \infty$ the Laplace transform of the Toeplitz matrix simplifies to

$$\tilde{\Sigma}^{\text{Toe}}(s) \simeq c\Gamma(\alpha + 1) \left(\frac{d}{s}\right)^{1+\alpha}. \quad (24)$$

While the Stieljes transform using Eq. (24) does not admit a closed form, we may gain some insight by studying the limit $\alpha \rightarrow 0$. Here, the sum takes the following form

$$S_d(\alpha \rightarrow 0) \simeq \sum_{s=1}^d \frac{1}{\frac{s}{cd} + \tilde{G}} = cd (H_{c\tilde{G}d+d} - H_{cd\tilde{G}}), \quad (25)$$

where $H(n)$ is the Harmonic number. Expanding for $d \rightarrow \infty$ the zeroth order result is

$$S_d(\alpha \rightarrow 0) \simeq cd \log \left(1 + \frac{1}{c\tilde{G}}\right), \quad (26)$$

leading to a closed form equation for $\tilde{G}(z)$ as

$$\tilde{G}(z) \simeq \frac{1}{-z + \gamma c \log \left(1 + \frac{1}{c\tilde{G}}\right)}, \quad (27)$$

and to the Stieljes transform

$$G(z) = -\frac{1}{c\gamma} \frac{1}{\left(1 + \gamma W\left(-\frac{1}{\gamma} e^{\frac{z-c}{c\gamma}}\right)\right)} + \frac{1-\gamma}{\gamma z}, \quad (28)$$

where $W(x)$ is the Lambert W function.

In Fig. 7, we show the theoretical results for the spectral density of a Wishart matrix with Σ^{Toe} covariance, for different values of α and c . For $\alpha \rightarrow -\infty$, the distribution is MP (shown in red). This distribution is bounded between λ_{\min} and λ_{\max} , and can only shift and expand depending on γ , insensitive to the correlations, which are vanishing. The black curves show the generalized MP distribution given by the inverse Stieljes transform of Eq. (28), for varying c . The distribution has a longer tail and depends on the correlation strength.